PAPER Nr.: 37

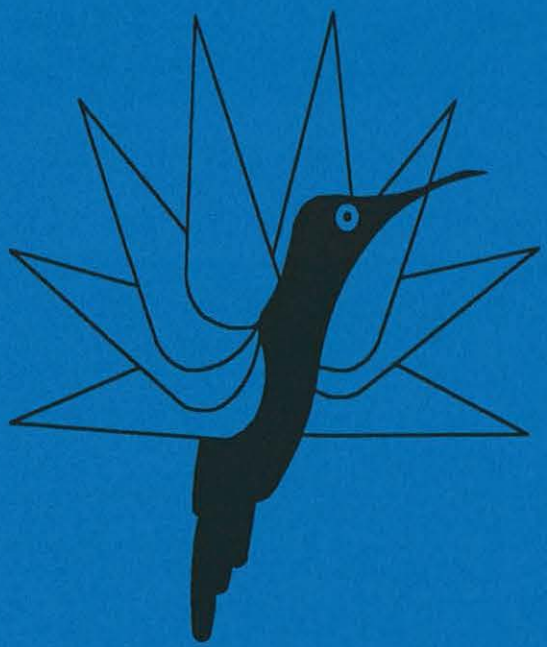

VORTEX-LATTICE FREE WAKE MODEL FOR HELICOPTER ROTOR DOWNWASH

BY

H. STAHL-CUCINELLI
EUROCOPTER DEUTSCHLAND GmbH
MÜNCHEN, GERMANY

TWENTIETH EUROPEAN ROTORCRAFT FORUM
OCTOBER 4 - 7, 1994 AMSTERDAM

Printed by the Technical Highschool Haarlem

VORTEX-LATTICE FREE WAKE MODEL FOR HELICOPTER ROTOR DOWNWASH

by
H. STAHL-CUCINELLI
EUROCOPTER DEUTSCHLAND GmbH, München, Germany

Abstract

A vortex-lattice method with a free-wake vortex model for the rotor downwash representation primarily used for 2-bladed rotors was extended to include 4-bladed rotors as well. In order to test the characteristic properties of the code, a parametric study has been done. It includes the investigation of panel and wake resolution. For receiving a smooth wake the introduction of a core radius is necessary. The airfoil thickness is taken into account by a correction of the lift coefficient. The results agree rather well with measurements for advance ratios of about 0.15.

1. List of Symbols

a_∞	- speed of sound
c	- blade chord
c_L	- lift coefficient
c_T	- thrust coefficient
DPt	- Data Point
M	- Mach number
M_{TH}	- hover tip Mach number
k(x,y)	- local blade vortex strength
n_r	- rotor rpm
nx	- chordwise panel number
ny	- spanwise panel number
r	- radial coordinate
rpm	- revolution per minute
R	- rotor blade radius
t	- time
th	- airfoil thickness
v_H, v_∞	- free stream velocity
w_i	- induced velocity
x,y,z	- cartesian coordinates
α_{TPP}	- tip path plane angle
α_s	- rotor shaft tilt angle
β_c	- pre-coning angle
γ	- vortex angular velocity
Γ	- blade section vortex strength
$\Theta_{0.7}$	- collective pitch angle at r/R=0.7
Θ_c	- lateral cyclic pitch angle
Θ_s	- longitudinal cyclic pitch angle
Θ_v	- twist angle
μ	- advance ratio
ρ	- air density
ψ	- azimuth angle
$\Delta\psi$	- azimuth step size
Ω	- rotor angular velocity

2. Theory

The lifting surface theory [1] is applied to the rotor flow. That is, the flow is supposed to be 3D, incompressible, inviscid and irrotational. For taking into account the blade thickness a correction [2] is applied:

$$\frac{C_L(th/c)}{C_L(th/c=0)} = 1 + 0.77 \cdot th/c$$

The most important property of the rotor flow is the unsteadiness. Its implementation will be demonstrated by a 2D model. Because the flow is irrotational the sum of the vortex strength Γ within a defined control volume has to be $\Sigma\,\Gamma = 0$ [3]. That is for $t = 0$ (valid for steady and unsteady flow):

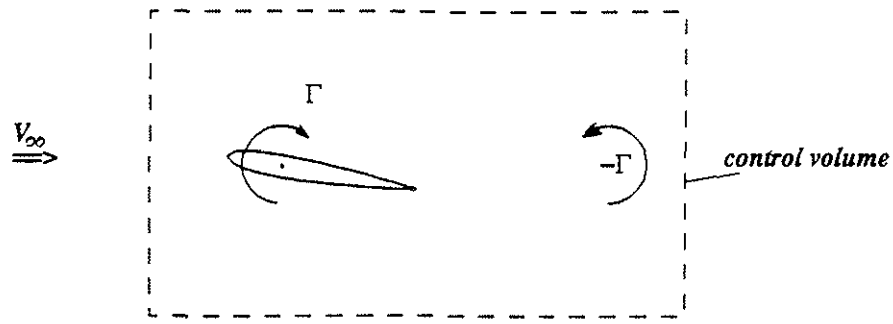

Fig. 1: *Vortex distribution in a control space at t = 0*

For the unsteady flow at $t = t + \Delta t$, an additional vortex is generated on the airfoil and an opposite rotating one must appear in the wake for conservation of the irrotationality.

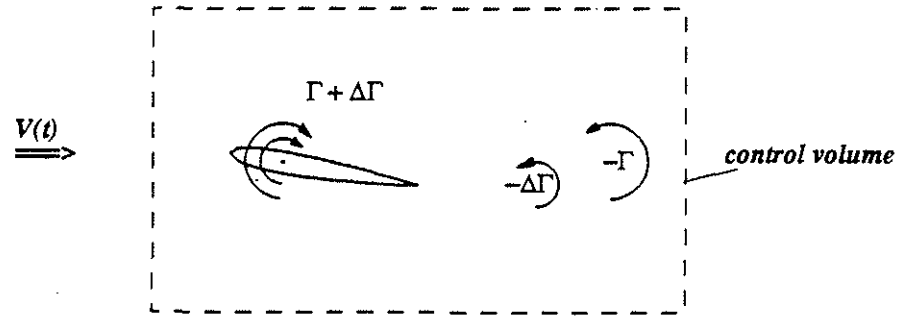

Fig. 2: Vortex distribution in a control space at $t = t + \Delta t$

The vortex strengths Γ of the blades are to be determined at each time step Δt by solving the system of equation resulting from the condition: $V(t) \cdot dn(t) = 0$.

3. Computational Model

The rotor blades are considered to move with the angular velocity Ω around the rotor axis while the velocity of the whole rotor is V_H caused either by the helicopter motion or by the wind tunnel speed.

Applying the theory above, the vortex strength $\Gamma(y) = \int k(x,y) \cdot dx$ is computed for each blade, separately. At each time step $t = t + \Delta t$ a new $\Gamma(y,\psi)$ together with a new wake panels leave the trailing edge of the blade when the rotor steps forward by $\Delta\psi$, see Figure 3.

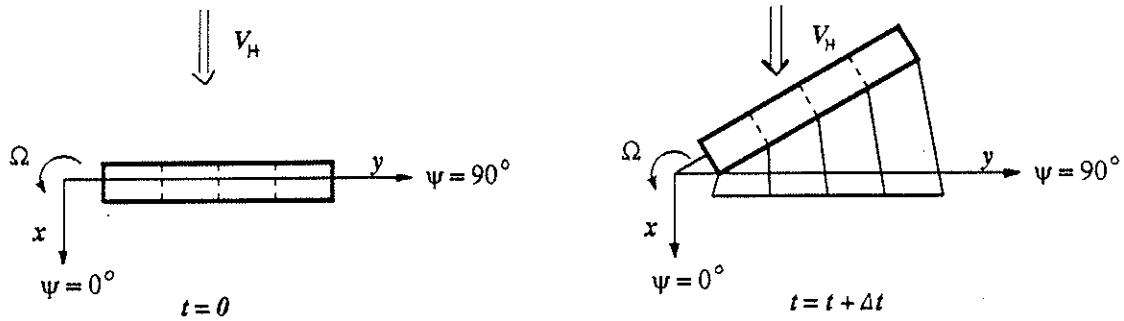

Fig. 3: Generation of new wake panels at t = 0

The positon of the wake panels has to be recomputed at each time step from the velocity V_H and the induced velocities w_i due to the blades and the wake vorticity. The velocity seen by the blades is changed by the wake influence. With these new boundary conditions the $\Gamma(y,\psi)$ can be recomputed, a.s.o.

A converged solution is obtained when the difference of flow properties from one cycle to the next tends to zero.

4. Measurements

For validating the code, measurements are used from the test campagne in the DNW done within the frame of the BRITE/EURAM research programme HELINOISE [4]. The test were done on the BO 105 4-bladed main rotor model with NACA 23012 airfoil. The rotor radius is R = 2m with a twist of Θ_v = -8°. The blades are rectangular (chord = 0.121 m) and the blade cut out is up to r/R = 0.182. The preconing angle is β_c = 2.5°. Test cases refered to herein are

- low-speed level flight (DPt 344)
- low-speed 6°-descent (DPt 1333)
- highest tip-speed 3°-descent (DPt1839)

Table 1 shows the test conditions for these three cases.

DPt	V_H	a_∞	ρ	μ	α_s	α_{TPP}	n_r	C_T	$\Theta_{0.7}$	Θ_c	Θ_s
	[m/s]	[m/s]	[kg/m³]		[°]	[°]			[°]	[°]	[°]
344	32.75	336.22	1.231	0.151	-0.95	-2.5	1034	.00446	5.35	1.58	-1.48
1333	32.63	338.57	1.255	0.149	5.05	3.5	1041	.00448	3.83	1.68	-1.01
1839	78.59	341.64	1.210	0.337	-8.97	-9.3	1099	.00458	10.32	-0.56	-3.84

* Heyson-type wind tunnel correction applied to α_s [5]

Table 1: Wind tunnel and rotor conditions

Test results are instantaneous pressure and noise data. The pressure values used herein are averaged over several revolutions. The samples were done at 2024 azimuthal positions per cycle.

At r/R = 0.75 and 0.97, the pressures were taken at 27 positions on the upper side and 17 positions on the lower side. At r/R = 0.87 there exist 14 pressure holes on the upper side and 10 on the lower side. At r/R = 0.6, 0.7, 0.8, 0.9 and 0.94, there is only one pressure hole on upper and lower side, respectively [4].

5. Parametric Study

The following parametric study is performed on the datapoint 344, if not otherwise indicated.

5.1 Convergence

When considering convergence the position of the starting vortex at t = 0 is important. This vortex from the blade at $\psi = 180°$ (at t = 0) is the last one that leaves the rotor disc area. Convergence can be expected when the starting vortices are moved more than one rotor diameter downstream of the rotor.

When $t_{min} = 2R / V_H$ is the minimum time at which this vortex has moved 2R downstream and $t_{1R} = 2\pi/\Omega$ is the time for one revolution then the minimum number of cycles are $n = 2 \times t_{min} / t_{1R} = 4.2$ for DPt 344. In Figure 4 the development of the pressure differences vs ψ is shown over 3 revolutions.

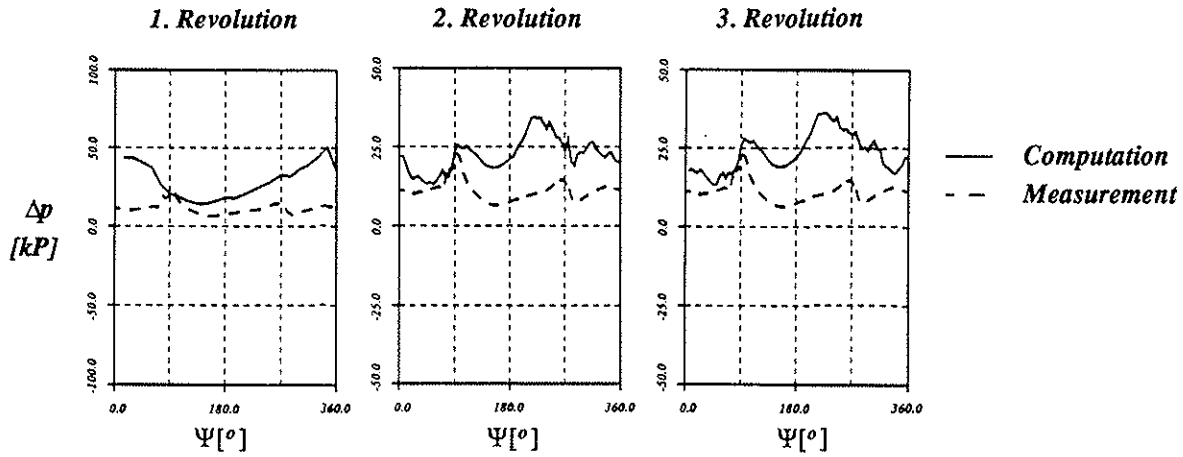

Fig. 4: Pressure differences vs ψ for 3 revolutions, r/R = 0.97, x/c = 0.21, NACA 0012

It can be seen that the difference between the 2nd and 3rd revolution is rather small. Changes occur mainly in the 1st and 4th quadrant of the rotor disc. There the influence of the starting vortices is still existent.

Because of high computing times the following investigations will already stop at the 2nd revolution. That seems to be sufficient for this parametric study.

5.2 Influence of Chordwise Resolution

The blades are panelled by nx panels chordwise and ny panels spanwise. The computation of the blade-vortex interaction and the blade pressure can be done with different panel numbers. For the following investigation the panel number for the pressure calculation is chosen to be $nx_p = 5$. The panel number nx_w for the interaction problem is varied, whereas the spanwise discretisation will remain unchanged (ny = 10).

In Figure 5, the influence of the chordwise panel number nx_W onto the pressure difference vs ψ is shown. Form this Figure, it can be concluded that one panel for generating the wake is insufficient. The characteristic shape of the curve will be approached with a minimum of $nx_W = 5$ panels.

In Figure 6, it will be seen that more panels nx_W are even more suitable. Here it should be noted that on the left there is $nx_W = 5$ and $nx_P = 5$ as above. Whereas on the right there is $nx_W = 10$ and $nx_P = 10$.

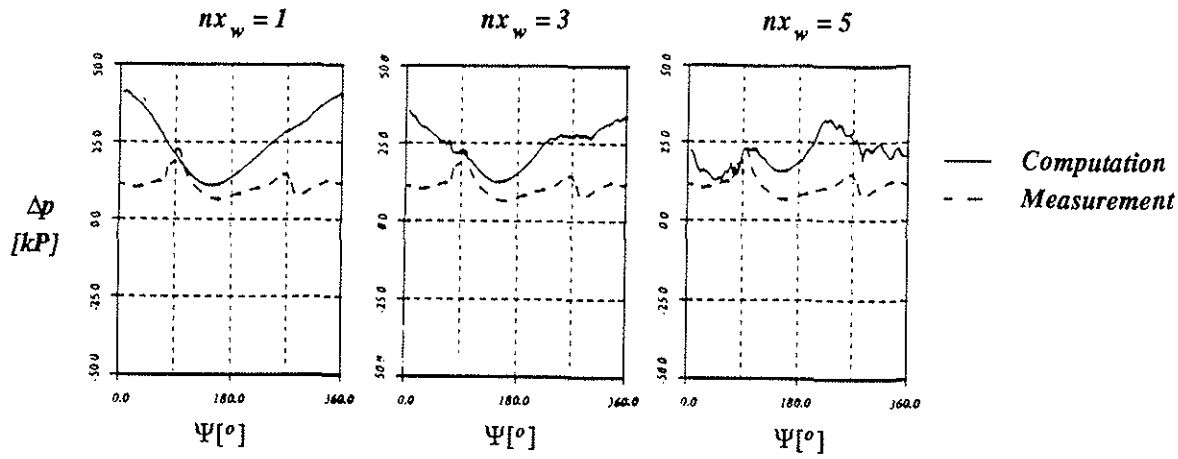

Fig. 5: Pressure differences vs ψ for several chordwise panel numbers nx_W, r/R = 0.97, x/c = 0.21, NACA 0012

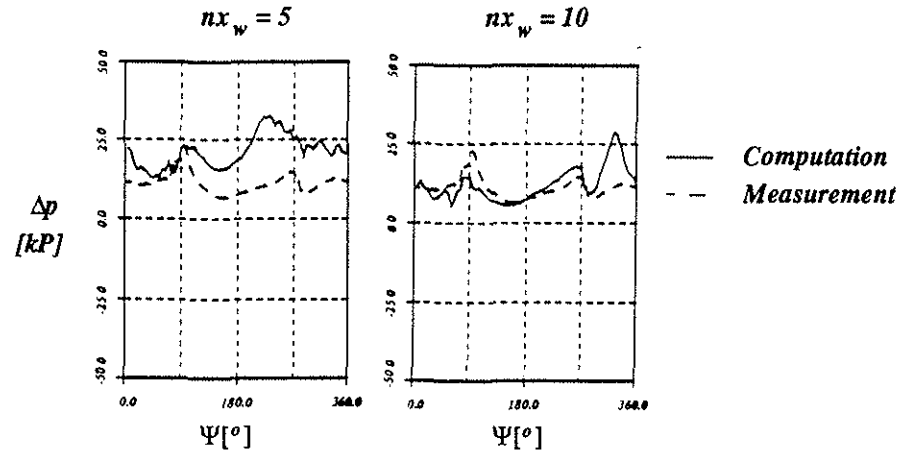

Fig. 6: Pressure differences vs ψ for chordwise resolution, r/R = 0.97, x/c = 0.21, NACA 0012

5.3 Influence of Spanwise Resolution

In the next step the influence of the spanwise panel number ny is considered. For this investigation the panel numbers nx and nx are chosen to be 5 and remain unchanged. In Figure 7, the influence of the spanwise panel number ny on the pressure difference vs ψ is shown.

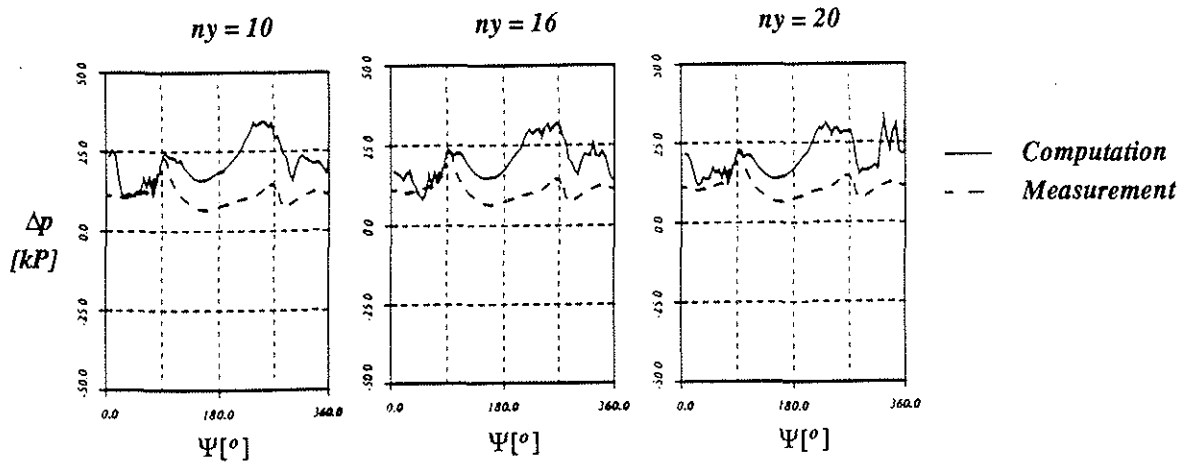

Fig. 7: Pressure differences vs ψ for spanwise resolution, r/R = 0.97, x/c = 0.21, NACA 0012

It can be seen that the more panels ny exist the more vortices can be resolved. Certainly, this is the result of a finer resolution of the wake. Now the panel numbers nx_p and nx_w are increased. They are chosen to be 10 and ny = 16. In Figure 8, the results are presented. As before, the pressure level decreases and the peaks around ψ = 90° and 270° seem to be smaller. However, they are increased in the 1st and 4th quadrant.

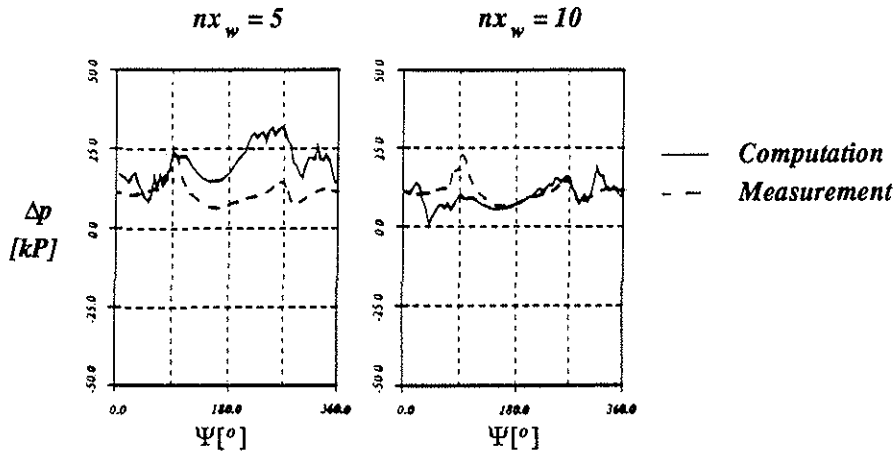

Fig. 8: Pressure differences vs ψ for chordwise resolution of $nx_P = nx_W = 5, 10$, ny = 16, r/R = 0.97, x/c = 0.21, NACA 0012

5.4 Azimuth Step Size

Another parameter of interest is the azimuth step size $\Delta\psi$ discretising the wake. The panel numbers are fixed to be nx = 5 and ny = 10. Four different step sizes are considered: $\Delta\psi$ = 5°, 10°, 15° and 20°.

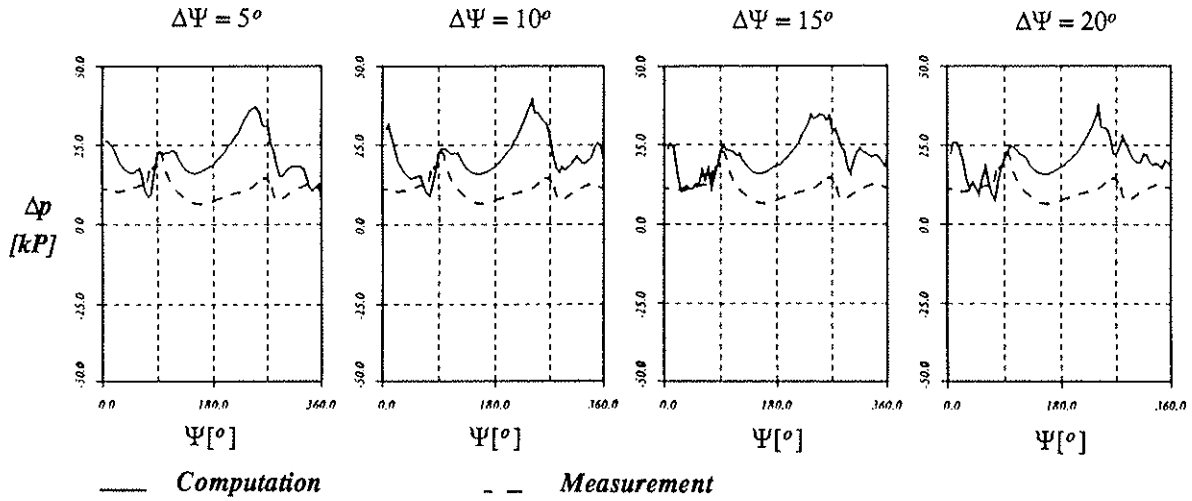

Fig. 9: Pressure differences vs ψ for azimuth step sizes, r/R = 0.97, x/c = 0.21, NACA 0012

Figure 9 shows the effect on the pressure difference. The main effect is a smoothing of the curve when reducing the step size. This effect results from a smoother geometric shape of the wake that appears at $\Delta\psi$ = 5° much more as a spiral then at $\Delta\psi$ = 20°. However, the CPU time exploses when reducing $\Delta\psi$. For $\Delta\psi$ = 20° the CPU time is about 1 hour. For $\Delta\psi$ = 5° the otherwise same test case takes about 48 hours on a Sun Sparc10.

5.5 Vortex Core Model

Because the wakes of the blades are free to move in space, they can pass very close to each other and the blades as well. The vortex is a potential vortex and its induced velocities tend to infinity when approaching the vortex core. However, in the viscous vortex core the induced velocity tend to zero, as can be seen in Figure 10.

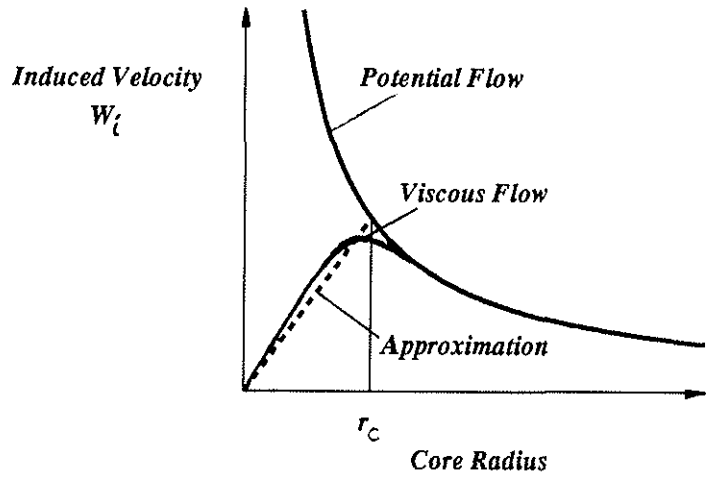

Fig. 10: Induced velocitiy of the potential and a viscous vortex

The high induced velocities of the potential vortex disturb the wake unrealistically strong. One way of getting around this is the introduction of an artificial core radius dependent on the angle γ. Whenever

$$\frac{\delta w_i}{\delta r} \geq \omega \qquad \omega = f(\gamma)$$

the approximation will be taken. The smaller γ the larger the core radius r_c will be. The effect of the angle representing the core radius is shown in Figure 11. At smaller γ that is at larger core radius r_c, the superposed pressure curve oscillations in the 1st and 4th quadrant caused by blade-vortex interaction are reduced.

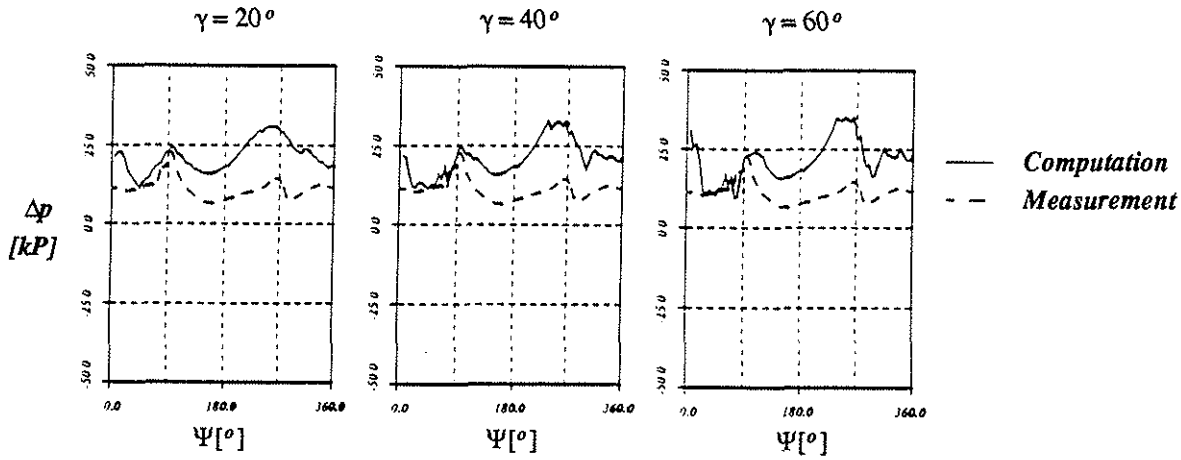

Fig. 11: Pressure difference vs ψ for several core radii, r/R = 0.97, x/c = 0.21, NACA 0012

5.6 Influence of the Rotor Tip Path Plane Angle

For comparison of computations and measurements the rotor shaft angle α_s of the wind tunnel test has to be corrected to free flight conditions. There are various theories taking into account tunnel effects. The tip path plane angles of Table 1 are corrected by Heyson's formula [5]. It is known that the more negative α_{TPP} the smaller is the interaction of the rotor blades and the wake. In order to get an idea how important a correct α_{TPP} for comparison with measurement is the corrected α_{TPP} = -2.5° is varied by ± 1.5°. The results are shown in Figure 12.

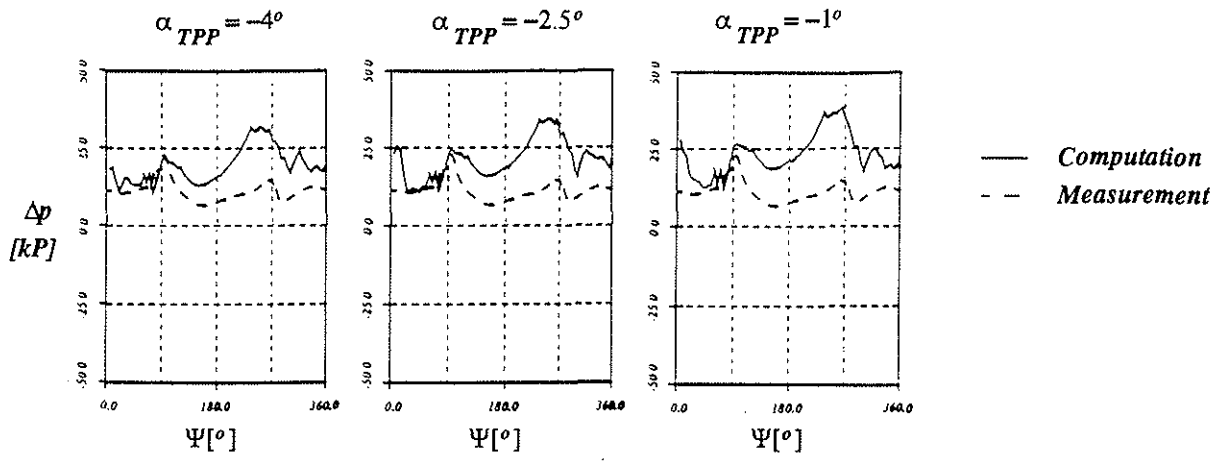

Fig. 12: Pressure differences vs ψ for different α_{TPP}, r/R = 0.97, x/c = 0.21, NACA 0012

It can be seen that as a result of a closer vicinity of the wake to the rotor disc (α_{TPP} = -1°), the peaks at ψ = 90° and 270° where strong blade-vortex interaction occur are higher. The general level of the curve is also higer than for α_{TPP} = -4°. It should be mentioned that the measurement shown correspond always to the case of α_{TPP} = -2.5° or α_s = -0.95°.

5.7 Influence of the Blade Airfoil

For all computations shown before the blade was considered to be a flat plate. The results are corrected for a thickness of 12 percent. So with respect to the lift and the vorticity strength, the blade was handled like a blade with NACA 0012 airfoil. Now the airfoil of the BO 105 rotor namely the NACA 23012 is introduced in the same way. The blade solution is as before: $nx_P = nx_W = 5$ and ny = 10 panels. The result is shown for the pressure distribution versus ψ in Figure 13.

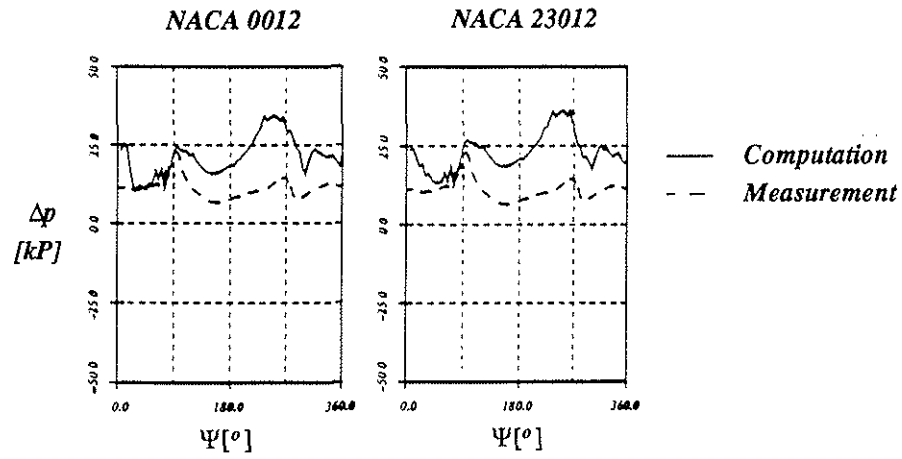

Fig. 13: Pressure difference vs ψ for two different airfoils, r/R = 0.97, x/c = 0.21

The influence of the NACA 23012 airfoil can be seen at a slightly higher pressure level especially at $\psi = 90°$. The global shape of the curve is almost unaffected.

6. Rearward Flow

At high advance ratios rearward flow can occur at the profiled inboard region of the retreating blade. On the thick airfoil the Kutta condition cannot be defined clearly because due to the nose radius there will separation appear. To handle the rearward flow the simplifying assumption will be made that the point corresponding to the trailing edge will be the nose point of the camber line for rearward flow.

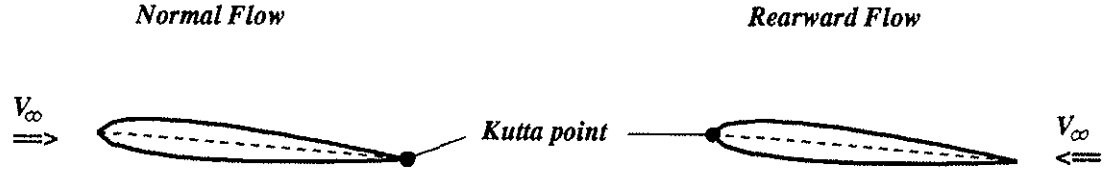

Fig. 14: Kutta condition for normal and rearward flow

For DPt 1839, $\mu = 0.337$, some part of the profiled blade is subjected to rearward flow. The results for the outer blade sections will not be considered because there are transonic effect which cannot be handled correctly with the potential theory. In Figures 15 and 16, the influence of the rearward flow is shown: Firstly, for the Kutta condition exclusively fulfilled at the trailing edge and, secondly, for the Kutta condition fulfilled either at the trailing or the leading edge depending on the flow direction (see Figure 17 for leading edge/trailing edge definition).

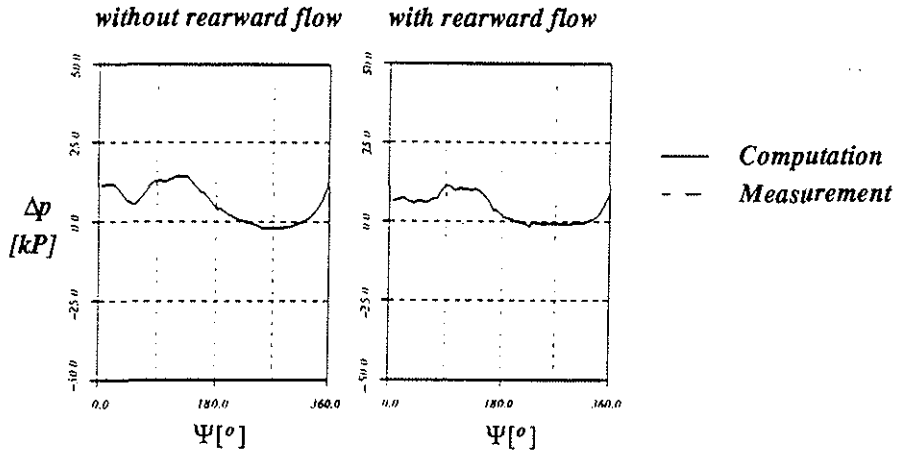

Fig. 15: Pressure differences vs ψ for r/R = 0.2, x/c = 0.21, NACA 0012

In Figure 15, the influence of the rearward flow on the pressure difference is shown. It can be seen that the region of influence is not restricted to the area around $\psi = 270°$ but also the flow at $0° < \psi < 90°$ is affected appreciably.

In Figure 16, the influence is shown for the pressure difference vs x/c for $\psi = 270°$. Without changed Kutta condition accounting for rearward flow the suction peak is at the leading edge. The pressure is not negative due to the angle of attack (really it is positive) but due to the inverse flow direction (rearward flow). Fulfilling the Kutta condition at the nose the suction peak occurs at the trailing edge. The pressure is negative because the angle of attack seen by the flow is negative, Figure 17.

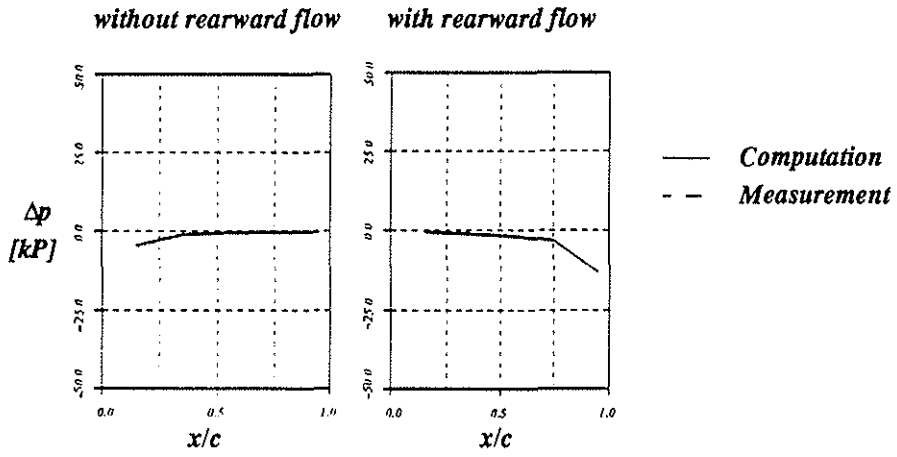

Fig. 16: Pressure differences vs x/c for r/R = 0.2, ψ = 270°, NACA 0012

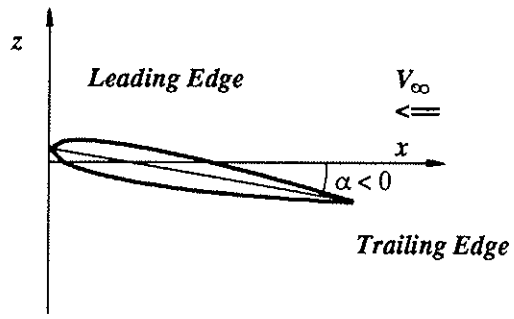

Fig. 17: Angle of attack for rearward flow

7. Computation for Data Point 1333

For a blade resolution of nx = 5 and ny = 10 panels for wake and pressure, respectively, the pressure difference for the DPt 1333 was computed and is shown in Figure 18 versus azimuth angle.

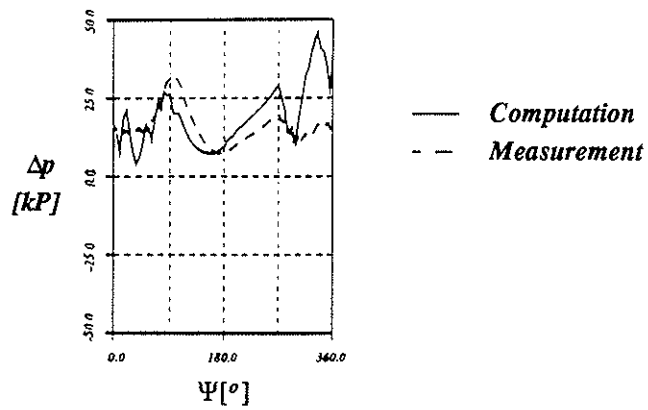

Fig. 18: Pressure difference vs ψ for DPt 1333, r/R = 0.97, x/c = 0.15, NACA 0012

DPt 1333 is a low-speed 6° descent flight case where the wake may penetrate the rotor disc more than at the level flight case DPt 344. The result shows good agreement between computation and measurement except on the 4th quadrant.

8. Conclusion

The parametric study on DPt 344 shows the following tendencies:

- Convergence
  Already after two revolutions the final shape of the pressure curve vs ψ is almost achieved. Only the global pressure level will be somewhat shifted and finer oscillation will change a bit. That means that the global wake stucture is defined after two revolutions. The position of the vortices will change only by small amounts.
- Blade surface resolution
  Generally, a higher resolution will improve the result. The chordwise panel number influences the wake shape dominantly. A number of 5 panels chordwise and 10 panels spanwise are sufficient for reliable results.
- Azimuth step size
  Reducing the azimuth step size $\Delta\psi$ (corresponding to the time step) smoothens the curve Δp versus ψ. A step size of 15 seems to be sufficient.
- Vortex core size
  As to be expected strong blade-vortex interaction will be reduced by larger vortex core sizes.
- Angle of tip path plane α_{TPP}
  The interaction of blades and vortices is more intensive as the vortex approaches the rotor disc. However, there is only a slight influence on the basic shape of the curve Δp versus ψ.
- Airfoil
  The two airfoils, NACA 0012 and NACA 23012, were applied. As expected, it could be shown that the NACA 23012 airfoil supplies more lift than the NACA 0012.

Furthermore, a model for rearward flow has been presented and was applied successfully.

The test case DPt 1333 for low speed descent was calculated. The computation and measurement agree rather well keeping in mind that the code really is restricted to incompressible and inviscid flow conditions.

9. References

1) Schlichting/Truckenbrodt, Aerodynamik des Flugzeuges (Teil II), Springer Verlag, Berlin/Heidelberg/New York, 1967

2) R. Padakannaya, The vortex lattice method for the rotor-wake interaction problem, NASA CR-2421, 1974

3) Schlichting/Truckenbrodt, Aerodynamik des Flugzeuges (Teil I), Springer Verlag, Berlin/Heidelberg/New York, 1967

4) P. Splettstoesser, B. Junker, K.-J. Schultz, W. Wagner, W. Weitemeyer, A. Protopsaltis, D. Fertis, The HELINOISE Aeroacoustic Rotor Test in the DNW - Test Documentation and Representative Results, DLR-Mitt. 93-09

5) H.H. Heyson, Use of Superposition in Digital Computers to Obtain Wind-Tunnel Interference Factors for Arbitrary ConFigurations, with Particular Reference to V/STOL Models. NASA TR R-302, 1969

6) A.Roettgermann, Ein Singularitaeten Verfahren zur Berechnung des Nachlaufs von Mehrblattrotorsystemen, Diplomarbeit Nr. 88/10, 1988

7) A. Roettgermann, R. Behr, Ch. Schoettl, S. Wagner, Calculation of blade vortex interaction of rotory wings in incompressible flow by an unsteady vortex lattice method including free wake analysis, paper presented at the GAMM-Symposium, Kiel, 1991

8) L. Zerle, S. Wagner, Influence of inboard shedded rotor blade wake to the rotor flow field, paper presented at 19th European Rotorcraft Forum, 1993